Near-Field Absorption in Prolate Spheroidal Models of Humans Exposed to a Small Loop Antenna of Arbitrary Orientation

AKHLESH LAKHTAKIA, MAGDY F. ISKANDER, MEMBER, IEEE, CARL H. DURNEY, MEMBER, IEEE, AND HABIB MASSOUDI, MEMBER, IEEE

Abstract— The power absorption characteristics of the prolate spheroidal model of an average man have been studied when the model is exposed to the near fields of an arbitrarily located small loop antenna. An integral equation is formulated and the fields radiated by the loop are expanded in terms of the vector spherical harmonics. This equation is then solved using the extended boundary condition method (EBCM).

For three different loop-spheroid configurations, the power distribution and the average SAR have been calculated as a function of the frequency and the separation distance. It is shown that the results obtained for separation distances larger than $\lambda/2$ agree well with those obtained from the plane wave exposure case. Furthermore, the average SAR values calculated as a function of separation distance for the case where the magnetic dipole moment is aligned parallel to the major axis of the spheroid are found to oscillate around the constant value obtained from the H-polarized plane wave exposure case. On the other hand, the average SAR values for the E-polarization case (magnetic dipole is parallel to the spheroidal minor axis) are found to increase monotonically with the decrease in separation distance. It is also shown that despite the complicated nature of the near fields, the absorption characteristics can still be explained in terms of the variations of the incident radiation. These loop results, together with those obtained from other simple soures [1], [2], can be used as building blocks in arriving at a qualitative understanding of the near-field absorption characteristics for more general exposure cases.

I. Introduction

MANY MEDICAL and industrial applications utilize radiofrequency sources operating at lower frequencies (typically, around 27 MHz). The near fields of these sources extend over large distances from the source, and hence the operating personnel are exposed mainly to near-field radiation. The hazardous effects due to these near fields, however, are different and less understood than those due to the extensively studied plane wave exposure. This is because of the complex characteristics of the near field, including the arbitrary angle between $\bar{E}$- and $\bar{H}$-fields, a wave impedance that is different from 377 Ω, and the general presence of the reactive energy components [3], [4]. Therefore there has recently been an increasing interest in the near-field absorption characteristics of biological objects.

In an attempt to study the absorption characteristics of near-field exposure, Iskander *et al.* [1], studied the exposure of a prolate spheroidal model to the near field of a short electric dipole. They observed that the average SAR oscillates about the plane wave results, and indicated possible SAR enhancement in the regions of small radii of curvature. Along the same lines, the same model was exposed to the near field of a small current loop antenna aligned coaxially about the major axis of the spheroid [2]. The distinguishing feature of the latter configuration is the absence of the electric field along the major axis, which results in significantly different radiation fields than those involved in the electric dipole case. From the coaxial loop results it was observed that there is no power absorbed along the major axis of the spheroid and that the heating is mainly confined to the vicinity of its surface. These results are of particular importance in hyperthermia, where extensive efforts are being directed towards achieving deep tissue heating by a coaxial coil carrying RF power at about 27 MHz [5]. Furthermore, in both of the above cases, it was possible to qualitatively explain the near-field absorption characteristics in terms of the characteristics of the incident fields.

In order to study the absorption characteristics of the block model of an average man being illuminated by realistic sources, the plane wave spectrum approach [6], [7] was used by Chatterjee *et al.* [8], to decompose the electric field, measured near a 27-MHz RF sealer, into an angular spectrum of plane waves, and the power distribution in the block model was calculated. It was observed that the SAR is not highly sensitive to spatial variations in the phase of the incident field, a result of major importance in near-field dosimetry since phase measurements are much more difficult than magnitude measurements to make. Their results also indicate that good estimates of the SAR may be obtained by using a convenient mathematical function to approximate the actual incident field distribution, which may itself be difficult to handle.

Although these results present a promising step towards analyzing the possible near-field effects, no general conclusions can be drawn from these simplified and special exposure cases. The characteristics of near fields vary greatly from source-to-source, since they depend on the specific dimensions and characteristics of their sources. Therefore, it is difficult to categorize these near fields and to classify their absorption characteristics. Consequently, it is very important to obtain as much qualitative understanding about the near-field absorption characteristics as

Manuscript received July 22, 1980; revised December 1, 1980.

The authors are with the Department of Electrical Engineering, University of Utah, Salt Lake City, UT 84112.

0018-9480/81/0600-0588$00.75 ©1981 IEEE

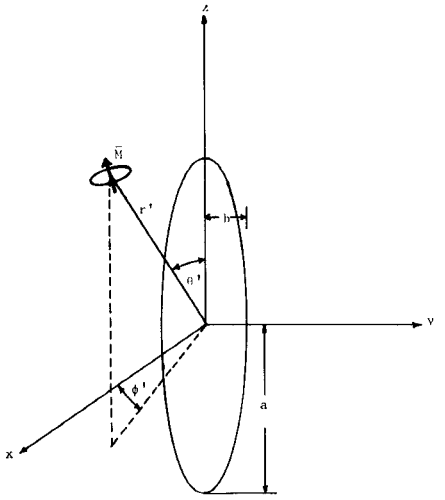

Fig. 1. Schematic diagram illustrating the position of the current loop source irradiating the spheroidal model; a and b are the semimajor and semiminor axes, respectively.

possible. If a few simple sources of sufficiently different, but exactly known, near fields are analyzed, general conclusions drawn from these analyses may be used as building blocks in arriving at a qualitative understanding of near-field absorption for more realistic and complicated irradiation conditions. We have undertaken the analyses of a few simple sources [1], [2], [9], and in this paper we describe the power absorbing characteristics of a prolate spheroidal model of an average man irradiated by the near field of an arbitrarily located small loop antenna. The problem is formulated in terms of an integral equation that involves the transverse dyadic Green's function. The fields radiated by the current loop are expanded in terms of the vector spherical harmonics, and the electromagnetic boundary value problem is solved using the extended boundary condition method (EBCM) [10].

II. Formulation

Consider a small loop carrying a constant current $I_0\exp(-j\omega t)$ and located at a point $\bar{r}'$ with respect to a prolate spheroidal model, as shown in Fig. 1. By using the equivalence principle, the fields induced inside the spheroid are replaced by their equivalent electric and magnetic surface current densities [11]. Therefore, upon applying the boundary conditions on the surface of the spheroid and equating the total fields in the interior of the model to zero, it is easy to obtain the following relationship between the incident electric field and the surface current densities [11]:

$$\nabla\times\int_S(\hat{n}\times\bar{E})\cdot\bar{G}(k\bar{r}|k\bar{r}')\,ds-\nabla\times\nabla\times\int_S\frac{1}{j\omega\epsilon_0}(\hat{n}\times\bar{H})\cdot\bar{G}(k\bar{r}|k\bar{r}')\,ds=-\bar{E}^i(\bar{r},\bar{r}') \quad (1)$$

where $\hat{n}$ is the unit outward normal on the surface S of the spheroid, and $(\hat{n}\times\bar{E})$ and $(\hat{n}\times\bar{H})$ are the equivalent magnetic and electric surface current densities on the surface S. $\bar{E}^i(\bar{r},\bar{r}')$ is the incident electric field at a point $\bar{r}$ due to the current loop located at $\bar{r}'$. The transverse dyadic Green's function $\bar{G}(k\bar{r}|k\bar{r}')$ is given by [12]

$$\bar{G}(k\bar{r}|k\bar{r}')=jk\sum_{n=1}^{\infty}\sum_{m=-n}^{n}\Big[\{h_n^{(1)}(kr')\bar{X}_{nm}(\theta',\phi')\}\cdot\{j_n(kr)\bar{X}_{nm}(\theta,\phi)\}+\frac{1}{k^2}\nabla\times\{h_n^{(1)}(kr')\bar{X}_{nm}(\theta',\phi')\}\cdot\nabla\times\{j_n(kr)\bar{X}_{nm}(\theta,\phi)\}\Big] \quad (2)$$

where $j_n(x)$ and $h_n^{(1)}(x)$ are, respectively, the spherical Bessel function and the spherical Hankel function of the first kind, and $\bar{X}_{nm}(\theta,\phi)$ is given by [13]

$$\bar{X}_{nm}(\theta,\phi)=\frac{1}{\sqrt{n(n+1)}}\bar{L}Y_{nm}(\theta,\phi) \quad (3)$$

where the operator $\bar{L}$ is defined as

$$\bar{L}\triangleq -j(\bar{r}\times\nabla)$$

$$Y_{nm}(\theta,\phi)=\sqrt{\frac{2n+1}{4\pi}\frac{(n-m)!}{(n+m)!}}\,P_n^m(\cos\theta)e^{jm\phi} \quad (4)$$

and $P_n^m(\cos\theta)$ is the associated Legendre function.

In order to reduce (1) to a system of simultaneous equations, it is necessary to expand the internal and the incident fields in terms of the vector spherical harmonics [14] and to apply the orthogonality properties of those functions. The unknown expansion coefficients of the internal fields are then determined by using the EBCM.

For a small current loop with magnetic dipole moment $\bar{M}$, it can be shown that the incident electric field is given by

$$\bar{E}^i(\bar{r},\bar{r}')=\frac{\eta_0}{4\pi}\sum_{n=1}^{\infty}\sum_{m=-n}^{n}\Big\{a_E(n,m)j_n(kr)\bar{X}_{nm}(\theta,\phi)-\frac{j}{k}a_M(n,m)\nabla\times\big[j_n(kr)\bar{X}_{nm}(\theta,\phi)\big]\Big\} \quad (5)$$

where the radial dependence takes into account that the spheroid lies wholly inside the sphere $r=r'$. The expansion coefficients $a_E(n,m)$ and $a_M(n,m)$ are given by [15]

$$a_E(n,m)=\frac{2\pi jk^3}{\sqrt{n(n+1)(2n+1)}}\bar{M}\cdot\left[\frac{(n+1)h_{n-1}^{(1)}(kr')}{\sqrt{2n-1}}\bar{\epsilon}^-+\frac{nh_{n+1}^{(1)}(kr')}{\sqrt{2n+3}}\bar{\epsilon}^+\right] \quad (6)$$

where

$$\epsilon_x^-=\big[(n+m)(n+m-1)\big]^{1/2}Y^*_{n-1,m-1}(\theta',\phi')-\big[(n-m)(n-m-1)\big]^{1/2}Y^*_{n-1,m+1}(\theta',\phi')$$

$$\epsilon_y^-=-j\Big\{\big[(n+m)(n+m-1)\big]^{1/2}Y^*_{n-1,m-1}(\theta',\phi')+\big[(n-m)(n-m-1)\big]^{1/2}Y^*_{n-1,m+1}(\theta',\phi')\Big\}$$

$$\epsilon_z^-=-2\big[(n+m)(n-m)\big]^{1/2}Y^*_{n-1,m}(\theta',\phi')$$

$$\epsilon_x^+ = [(n+m+1)(n+m+2)]^{1/2} Y^*_{n+1,m+1}(\theta',\phi') - [(n-m+1)(n-m+2)]^{1/2} Y^*_{n+1,m-1}(\theta',\phi')$$

$$\epsilon_y^+ = j\{[(n+m+1)(n+m+2)]^{1/2} Y^*_{n+1,m+1}(\theta',\phi') + [(n-m+1)(n-m+2)]^{1/2} Y^*_{n+1,m-1}(\theta',\phi')\}$$

and

$$\epsilon_z^+ = -2[(n+m+1)(n-m+1)]^{1/2} Y^*_{n+1,m}(\theta',\phi')$$

and

$$a_M(n,m) = \frac{2\pi jk^3}{\sqrt{n(n+1)}} h_n^{(1)}(kr')\bar{M}\cdot\bar{R} \tag{7}$$

where

$$R_x = [(n-m)(n+m+1)]^{1/2} Y^*_{n,m+1}(\theta',\phi') + [(n+m)(n-m+1)]^{1/2} Y^*_{n,m-1}(\theta',\phi')$$

$$R_y = j\{[(n-m)(n+m+1)]^{1/2} Y^*_{n,m+1}(\theta',\phi') - [(n+m)(n-m+1)]^{1/2} Y^*_{n,m-1}(\theta',\phi')\}$$

and

$$R_z = 2mY^*_{nm}(\theta',\phi').$$

The expansion in (5) can be expressed in a more convenient form by using the vector spherical wave functions $\bar{M}^1_{\sigma mn}$ and $\bar{N}^1_{\sigma mn}$ as defined by Stratton [14]. It is easy to show that the incident electric field is given in terms of these functions by

$$\bar{E}^i(\bar{r},\bar{r}') = j\frac{\eta_0}{4\pi}\sum_{n=1}^{\infty}\sum_{m=-n}^{n}\alpha_{nm} \cdot\{[a_E(n,m)\bar{M}^1_{emn} + a_M(n,m)\bar{N}^1_{omn}] + j[a_E(n,m)\bar{M}^1_{omn} - a_M(n,m)\bar{N}^1_{emn}]\} \tag{8}$$

where

$$\alpha_{nm} = (-1)^m \sqrt{\frac{2n+1}{4\pi}\frac{1}{n(n+1)}\frac{(n-m)!}{(n+m)!}}.$$

Similarly, the internal electric field is expanded in terms of the $\bar{M}^1_{\sigma mn}$ and $\bar{N}^1_{\sigma mn}$ functions as given by

$$\bar{E}^{\text{int}}(\bar{r},\bar{r}') = \sum_{n=1}^{\infty}\sum_{m=0}^{n} C_{\sigma mn}\bar{M}^1_{\sigma mn} + D_{\sigma mn}\bar{N}^1_{\sigma mn}, \quad \sigma = \begin{cases}\text{even}\\ \text{odd}\end{cases}. \tag{9}$$

Here, $C_{\sigma mn}$ and $D_{\sigma mn}$ are the unknown expansion coefficients, and are obtained by using the procedure outlined earlier in this section.

III. Numerical Procedure and Results

To obtain the expansion coefficients of the internal fields, the incident field expansion in (8) is programmed and used in (1). The program is considerably simplified, however, by choosing only specific locations for the loop.

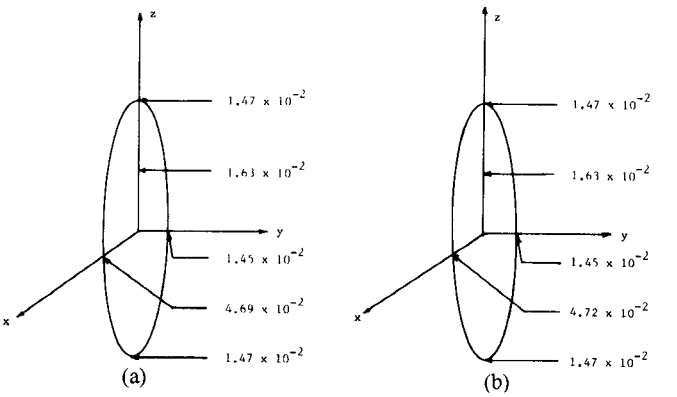

Fig. 2. Comparison between SAR distributions (W/kg) at 27 MHz for a man model. (a) Current loop located at $r'/\lambda > 2$, $\bar{M} = M_y\hat{y}$, $\theta' = 90°$, $\phi' = 0°$. (b) E-polarized plane wave radiation with incident power density of 1 mW/cm^2 [11].

If, for example, the loop is assumed to be located in the $\phi' = 0°$ plane, the terms involving $\sin m\phi'$ in the expansion coefficients $a_E(n,m)$ and $a_M(n,m)$ reduce to zero. This assumption does not limit the generality of the problem since the prolate spheroidal model is symmetrical around the z axis, and so the calculations are not affected by the choice of a specific $\phi' =$ constant plane. Similarly, if θ' is given the value of 90°, it is easier to calculate the spherical harmonics. The particular value of θ' is chosen so as to correspond, if applicable, at large values of r'/λ, to the E- or H-polarizations for the incident plane wave case [16].

A computer program to solve for the internal field coefficients on the UNIVAC 1108 computer was written, and the SAR distribution and the average SAR values were calculated at different frequencies for the prolate spheroidal model of an average man ($a = 0.875$ m and $a/b = 6.34$). Relevant information about the complex permittivity of the model as a function of frequency was obtained from the *Radiofrequency Radiation Dosimetry Handbook* [17].

The SAR at any point $\bar{r}$ inside the spheroid is calculated as

$$\text{SAR}(\bar{r}) = \frac{1}{2}\sigma|\bar{E}^{\text{int}}(\bar{r},\bar{r}')|^2 \tag{10}$$

where σ is the conductivity of the model. The average SAR, on the other hand, is obtained by integrating the absorbed power distribution over the volume of the spheroid and taking advantage of the symmetry conditions.

Consider the case where the loop is located at $\phi' = 0°$ and $\theta' = 90°$, and that the magnetic dipole moment $\bar{M}$ is oriented along the y-direction (i.e., the loop is contained in the x–z plane). This irradiation condition at large r'/λ corresponds to the case of the E-polarized incident plane wave. The SAR distribution obtained for this case at large r'/λ is compared with the E-polarized plane wave case in Fig. 2. In the results given in Fig. 2, the dipole moment $\bar{M}$ is normalized so that the average SAR values obtained for a loop at large distance from the spheroid are equal to those values obtained from the plane wave irradiation case with incident power density equal to 1 mW/cm^2. This normalization constant does not affect the relative distri-

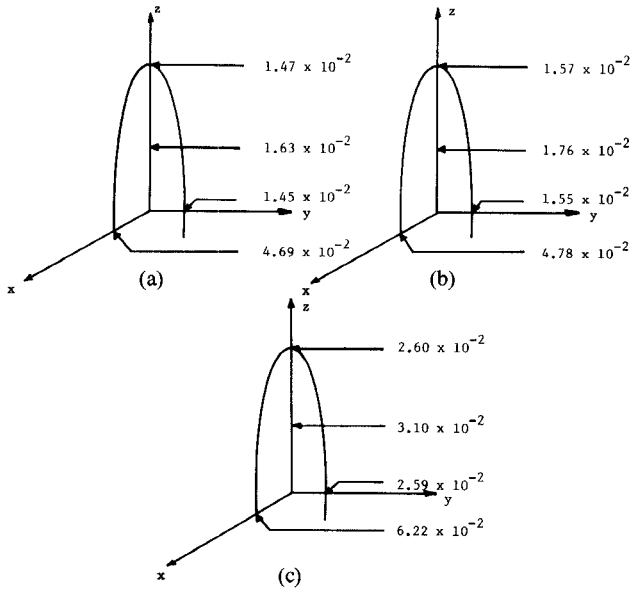

Fig. 3. SAR distribution (W/kg) in a spheroidal model of man at 27 MHz and as a function of loop location. $\underline{M}=M_y\hat{y}$, $\theta'=90°$, $\phi'=0°$. (a) $r'/\lambda=2.0$. (b) $r'/\lambda=0.5$. (c) $r'/\lambda=0.15$.

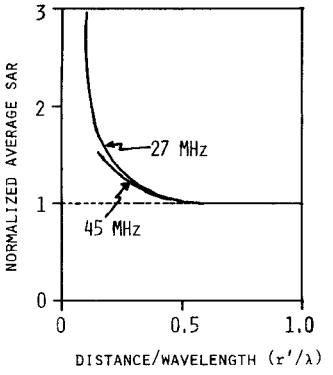

Fig. 4. Normalized average SAR values for a spheroidal model of man at 27 MHz and 45 MHz. The loop has a magnetic dipole moment $\underline{M}=M_y\hat{y}$ and is located at $\theta'=90°$ and $\phi'=0°$. The SAR values are normalized with respect to their plane wave value.

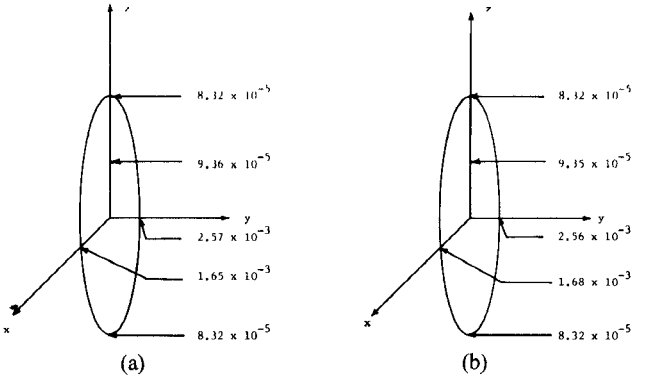

Fig. 5. Comparison between SAR distributions (W/kg) at 27 MHz for a man model. (a) Current loop located at $r'/\lambda>2$, $\underline{M}=M_z\hat{z}$, $\theta'=90°$, $\phi'=0°$. (b) H-polarized plane wave radiation with incident power density of 1 mW/cm^2 [11].

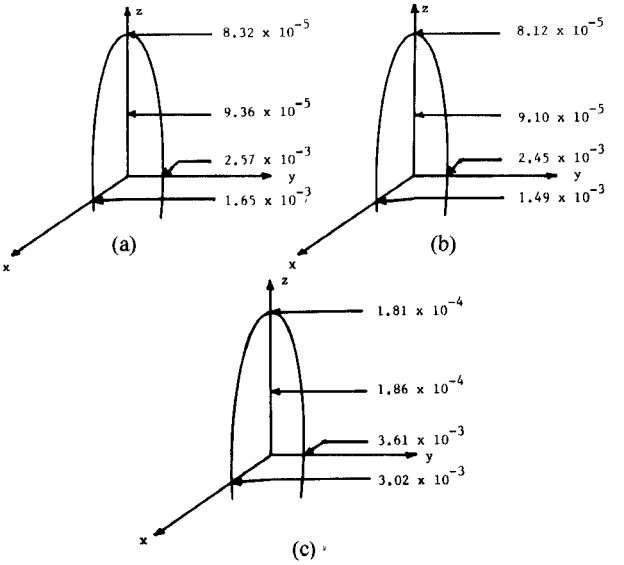

Fig. 6. SAR distribution (W/kg) in a spheroidal model of man and as a function of loop location. $\underline{M}=M_z\hat{z}$, $\theta'=90°$, $\phi'=0°$. (a) $r'/\lambda=2.0$. (b) $r'/\lambda=0.5$. (c) $r'/\lambda=0.15$.

bution since it is used only to scale the absorbed power values. Furthermore, since the far-field radiated power density is inversely proportional to the square of the distance from the loop, the normalization constant is also used to eliminate this distance dependence in this comparison. This procedure thereby ensures that the resulting differences, if any, can be attributed to the reactive energy existing in the near zone.

The power distribution in a spheroidal model of an average man is shown in Fig. 3 for different separation distances r'/λ at 27 MHz. At this frequency the complex permittivity is $\epsilon'=78.5$ and $\epsilon''=270.0$. From Fig. 3 it is clear that at large r'/λ the distribution is similar to that of the corresponding E-polarized plane wave case [16], while significant variations are observed for very small values of r'/λ.

The average SAR values are plotted, in Fig. 4, as a function of the normalized separation r'/λ for the man model. It should be noted that the average SAR for $r'/\lambda>0.5$ has almost the plane wave value because of the normalization procedure outlined above. Furthermore, the average SAR continues to increase with the decrease of the normalized distance r'/λ.

For the second case, the loop is assumed to be located at $\phi'=0°$ and $\theta'=90°$ and is oriented in the x–y plane so that the magnetic dipole moment $\underline{M}$ points in the z direction. At large values of r'/λ, this orientation corresponds to that of H-polarization for an incident plane wave case [16]. Fig. 5 compares the power distribution in the model of an average man when it is exposed to a current loop oriented as described above and to an incident H-polarized plane wave of power density 1 mW/cm^2. The dipole moment is scaled in order to correspond to the plane wave case at large separation distances.

The SAR distributions in the model of an average man are shown in Fig. 6 at 27 MHz for different separation distances. It is clear that although the distribution is similar to the corresponding plane wave SAR distribution at

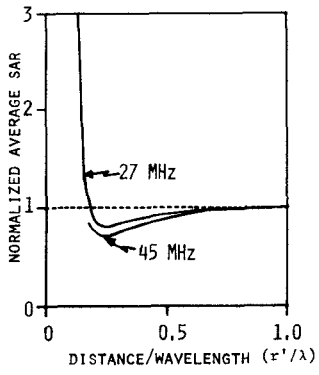

Fig. 7. Normalized average SAR values for a spheroidal model of man at 27 MHz and 45 MHz. The loop has a magnetic dipole moment $\bar{M}=M_z\hat{z}$ and is located at $\theta'=90°$ and $\phi'=0°$. The SAR values are normalized with respect to their plane wave value.

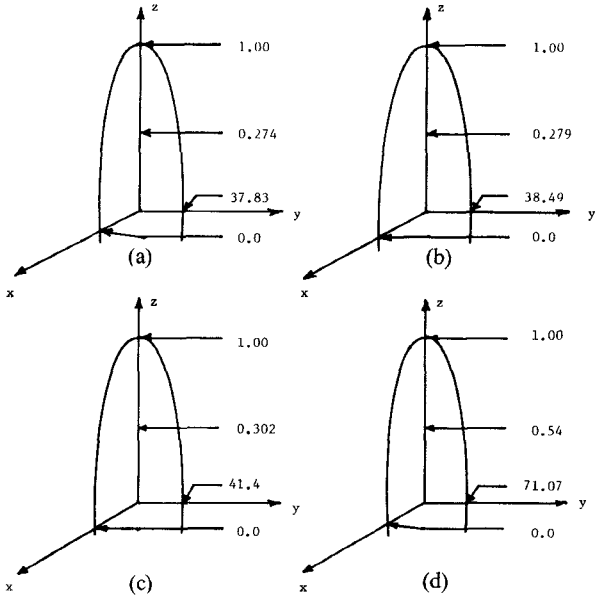

Fig. 8. Normalized SAR (W/kg) distribution in a spheroidal model of man at 27 MHz as a function of the separation distance r'. The magnetic dipole moment of the loop is $\bar{M}=M_x\hat{x}$ and the loop location is $\theta'=90°$ and $\phi'=0°$. (a) $r'/\lambda=2.0$. (b) $r'/\lambda=1.0$. (c) $r'/\lambda=0.5$. (d) $r'/\lambda=0.2$.

large r'/λ, significant variations are observed for shorter separation distances. The average SAR values are plotted against the normalized distance r'/λ in Fig. 7, where it may be seen that for $r'/\lambda>0.5$, the average SAR agrees with the plane wave value. As the value for r'/λ continues to decrease further, the average SAR first drops to a minimum and then continues to increase monotonically.

Finally, the loop is assumed to be located at $\phi'=0°$ and $\theta'=90°$ and oriented such that the magnetic dipole moment is along the x direction. Consequently, the magnetic dipole is aligned along a minor axis of the spheroid. The normalized SAR distributions in the man model are shown in Fig. 8, at 27 MHz and for different separation distances. From this figure it is clear that no power is absorbed along the x axis because the electric field along this axis is zero, and most of the power is absorbed in the lateral regions of the model. The latter simply results in an SAR enhancement at the two ends of the major axis of the spheroid. Power absorption in the lateral regions, in relation to the rest of the model, becomes more pronounced as the normalized separation distance r'/λ decreases. It should also be noted that for separation distances larger than $\lambda/2$, the SAR distribution agrees with the far-field SAR distribution.

IV. Discussion and Conclusions

The absorbed power distribution in and the average SAR values of the prolate spheroidal model of an average man irradiated by the near field of a small loop antenna are presented.

Three different orientations of the loop are considered and the SAR results of each are compared with the corresponding plane wave polarization. It is shown that the average SAR values for loops located at large distances ($r'/\lambda>0.5$) from the spheroid agree well with their plane wave counterparts. For smaller values of the separation distance r'/λ, however, the power distribution and the average SAR values differ significantly from the far-zone results. This is due to the presence of the reactive energy components in the near field.

For the E-polarized current loop case ($\bar{M}=M_y\hat{y}, \theta'=90°, \phi'=0°$), it is shown that the average SAR increases continuously as the separation distance decreases. This contrasts markedly with the oscillations in the average SAR profile reported for the E-polarized electric dipole [1]. The reason for the initial reduction, observed in the electric dipole case as r'/λ decreases, is explained as being due to the presence of the radial electric field component E_r in the near field of the short electric dipole. This electric field component is weakly coupled since it is perpendicular to the surface of the spheroid [1]. In the present loop case, on the other hand, the average SAR values increased continuously with the decrease in the separation distance. This can be explained in terms of the presence of the additional radial magnetic field component H_r in the near field of the loop. The coupling between this field component and the spheroid has been shown to be related to the maximum cross-sectional area the model presents normal to the direction of H_r [2]. Therefore, when this area is small, the coupling is said to be weak and the average SAR has a low value. Strong coupling occurs when this area is large, and then the average SAR has a high value. For the E-polarized current loop case, H_r is perpendicular to the major axis of the spheroid, and is, therefore, strongly coupled. This accounts for the continuous increase in the average SAR values as the value of r'/λ decreases.

The calculated relative values of the electric and the magnetic fields radiated by a small current loop are plotted in Fig. 9 as a function of distance at 30 MHz. It is interesting to note that the variation of the normalized average SAR values as a function of r'/λ, as shown in Fig. 4, is similar to the variation of the incident E-field of the current loop plotted as a function of the normalized distance (λ/x) in Fig. 9. This agrees with the qualitative understanding obtained from numerical calculations [18],

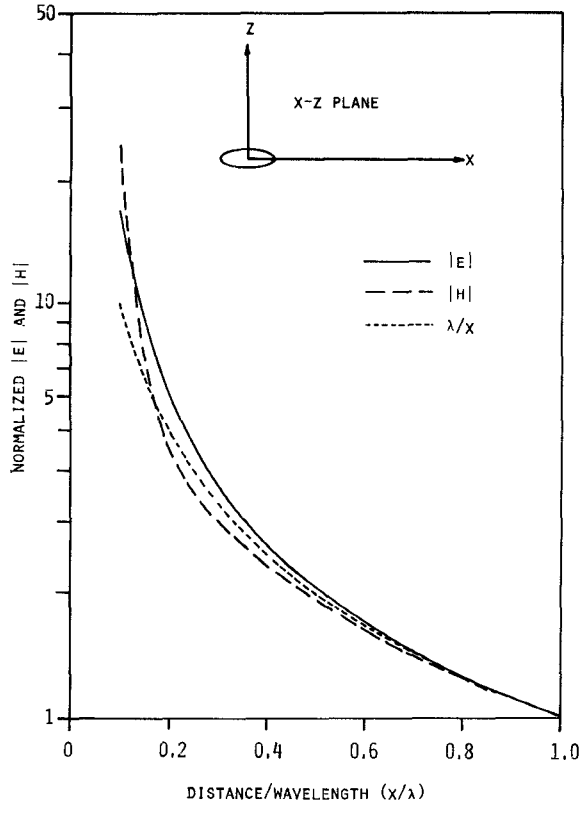

Fig. 9. Calculated relative values of fields versus normalized distance for a current loop at 27 MHz, at a point $z=30$ cm in the x–z plane.

according to which the contribution of the incident E-field dominates over the contribution of the incident H-field for cases where the incident E-field is parallel to the major axis of the spheroid.

In the second case, where the loop is located at $\phi'=0°$ and $\theta=90°$ and has a magnetic dipole moment parallel to the z axis, it was shown that the average SAR first falls to a minimum (below the plane wave value) and then increases to values above the plane wave result. This behavior of oscillations about the plane wave result is similar to that in the E-polarized electric dipole case [1].

It has been shown from numerical computations [18] that for the case of the incident H-field being parallel to the major axis of the prolate spheroidal model, the contribution of the incident H-field is the dominant contribution. Hence, for the H-polarized current loop case ($\overline{M}=M_z\hat{z}, \theta'=90°, \phi'=90°$), the variation of the normalized average SAR values as a function of r'/λ, as shown in Fig. 7, is similar to the variation of the incident magnetic field strength plotted as a function of the normalized distance in Fig. 9. This accounts for the oscillation of the average SAR values about the plane wave result for this loop case.

Thus it is seen that in spite of the complex nature of the near field of the small current loop, it is possible to qualitatively explain the near-field power absorption characteristics in terms of the variations of the incident fields. This conclusion has also been observed in our other near field analyses [1], [2], [9], the matter which suggests its generality.

The problem of obtaining convergent solutions for the SAR distribution, which has been previously encountered for near-field irradiation by a short electric dipole [1] and for plane wave illumination of prolate spheroids [16], occurred for the case of the current loop, too. The matrix size for a given frequency and the number of values of m considered increased with the decrease of the separation distance r'/λ because more terms were required to calculate the reactive energy components accurately.

However, at small separation distances $r'/\lambda<0.5$, the problem of obtaining convergent solutions became even more acute. This is because the solution of (1) is convergent only inside the largest sphere inscribed in the spheroid, where the total fields were equated to zero [11]. Therefore, the results are not accurate throughout the rest of the spheroid; and the inaccuracy increases as the observation point becomes more distant from the center of the sphere of convergence, so that the least accurate results appear at the two ends of the model.

In order to overcome this problem, we need to guarantee null fields throughout the interior volume of the spheroid. The procedure devised by Waterman [10] (and subsequently used by others [1], [16]) assures a convergent solution by utilizing the concept of analytic continuation. In brief, if an analytic function can be expanded within a region of finite radius of convergence, then it is possible to expand the same function about any origin within the original region of convergence out to the nearest singularity of the function. This process can be repeated, thereby resulting in the analytic continuation of the function from its original region of convergence to other parts of the total volume being considered. In the present problem, the original sphere of convergence is the inscribed sphere of the spheroid; and, its center was continuously shifted along the z axis, so that a convergent solution was obtained, section by section, throughout the interior of the model.

References

[1] M. F. Iskander, P. W. Barber, C. H. Durney, and H. Massoudi, "Near-field irradiation of prolate spheroidal models of humans," *IEEE Trans. Microwave Theory Tech.*, vol. MTT-28, pp. 801–807, 1980.

[2] A. Lakhtakia, M. F. Iskander, C. H. Durney, and H. Massoudi, "Irradiation of prolate spheroid models of humans and animals in the near field of a small loop antenna," *Radio Sci.*, Dec. 1980.

[3] D. L. Conover, W. H. Parr, E. L. Sensintaffar, and W. E. Murray, Jr., "Measurement of electric and magnetic field strengths from Industrial Radiofrequency (15-40.68 MHz) power sources", HEW publication (FDA) 77-8011, C. C. Johnson and M. L. Shore, Eds., Dec. 1976.

[4] P. F. Wacker and R. R. Bowman, "Quantifying hazardous electromagnetic fields: Scientific basis and practical considerations," *IEEE Trans. Microwave Theory Tech.*, vol. MTT-19, pp. 178–187, 1971.

[5] F. K. Storm, W. H. Harrison, R. S. Elliott, and D. L. Morton, "Hyperthermia in cancer treatment: Normal tissue and solid tumor effects in animals models and clinical trials," presented at the American Cancer Society Symp., San Diego, CA, Sept. 15–16, 1978.

[6] H. G. Booker and P. C. Clemmow, "The concept of an angular spectrum of plane waves and its relation to that of polar diagram and aperture distribution," *Proc. Inst. Elect. Eng.*, vol. 97, part III, pp. 11–17, 1950.

[7] P. C. Clemmow, *The Plane Wave Spectrum Representation of Electromagnetic Fields*. New York: Pergamon, 1956.

[8] I. Chatterjee, M. J. Hagmann, and O. P. Gandhi, "Electromagnetic energy deposition in an inhomogeneous block model of man for near-field irradiation conditions," accepted for publication by *IEEE*

Trans. Microwave Theory Tech., vol. MTT-28, pp. 1452–1459, 1980.
[9] M. F. Iskander, H. Massoudi, C. H. Durney, and S. J. Allen, "Measurements of the RF power absorption in spheroidal human and animal phantoms exposed to the near field of a dipole source," accepted for publication in *IEEE Trans. Biomed. Eng.*, vol. BME-28, Mar. 1981.
[10] P. C. Waterman, "Symmetry, unitarity, and geometry in electromagnetic scattering," *Phys. Rev. D*, vol. 3, pp. 825–839, 1971.
[11] P. W. Barber and C. Yeh, "Scattering of electromagnetic waves by arbitrary shaped dielectric bodies," *Appl. Opt.*, vol. 14, pp. 2864–2872, 1975.
[12] P. M. Morse and H. Feshbach, *Methods of Theoretical Physics*. New York: McGraw-Hill, 1953.
[13] J. D. Jackson, *Classical Electrodynamics*. New York: Wiley, 1962.
[14] J. A. Stratton, *Electromagnetic Theory*. New York: McGraw-Hill, 1941.
[15] H. Chew, P. J. McNulty, and M. Kerker, "Model for Raman and fluorescent scattering by molecules embedded in small particles," *Phys. Rev. A*, vol. 13, pp. 396–404, 1976.
[16] P. W. Barber, "Resonance electromagnetic absorption by nonspherical dielectric objects," *IEEE Trans. Microwave Theory Tech.*, vol. MTT-25, pp. 373–381, 1975.
[17] C. H. Durney, C. C. Johnson, P. W. Barber, H. Massoudi, M. F. Iskander, J L. Lords, D. K. Ryser, S. J. Allen, and J. C. Mitchell, *Radiofrequency Radiation Dosimetry Handbook*, 2nd ed., Depts. Electrical Engineering and Bioengineering, Univ. of Utah, Salt Lake City, 1978.
[18] C. H. Durney, M. F. Iskander, H. Massoudi, A. Lakhtakia, J. Han, P. W. Barber, and H. C. Chen, "Comparison of theoretical and experimental absorption of radiofrequency power," University of Utah, Dep. Electrical Engineering, Salt Lake City, UT, Third Quarterly Rep. F33615-79-C-0614, Jan. 1980.

Reflection by a Sinusoidally Modulated Surface Reactance at Oblique Incidence

S. R. SESHADRI, SENIOR MEMBER, IEEE

Abstract—**The reflection characteristics of the TM and the TE surface waves by a weak sinusoidal modulation of the surface reactance are investigated for the oblique incidence in which the wavevectors are not aligned with the grating vector. A superposition of TM and TE wave fields is needed for the fulfillment of the required boundary conditions. For both the TM and the TE surface waves, the Brewster phenomenon of total transmission occurs at the angle of incidence $\theta=\theta_B=45°$. A modulation in the surface reactance, in general, causes the TE surface waves to be more efficiently reflected than the TM surface waves.**

I. Introduction

THE WAVE PROPAGATION in a structure having a spatially periodic variation of its physical parameters is a subject of increasing importance in connection with grating couplers, filters, and distributed feedback oscillators [1]. A majority of the investigations in this field have considered only the special case of normal incidence in which the wavevectors are parallel to the grating vector. The general case of oblique incidence in which the wavevectors are not aligned with the grating vector is important in integrated millimeter wave and optical circuits in view of its applications such as Bragg deflectors [2], chirped-grating demultiplexers [3], and tunable distributed feedback oscillators [4]. An important feature of the oblique incidence is the need to use a superposition of transverse magnetic [TM] and transverse electric [TE] wave fields for the fulfillment of the required boundary conditions. In this paper a rigorous technique is developed for a systematic treatment of the coupling of the TM and the TE modes.

A thin dielectric waveguide having a spatially periodic variation of its permittivity or thickness can be modeled by a reactance surface having a spatially periodic variation of its surface reactance [5]. The reflection characteristics of the TM surface waves by a sinusoidal modulation in the surface reactance have been investigated previously for the special case of normal incidence [5], [6]. In this paper, the reflection characteristics of the surface waves by a sinusoidal modulation in the surface reactance are treated for the general case of oblique incidence in which the wavevectors are inclined at an angle to the grating vector. The statement of the problem is given in Section II. In Sections III and IV the TM and the TE surface waves are treated, respectively. In Section V the important results are summarized.

Manuscript received September 30, 1980; revised December 19, 1980.
The author is with the Department of Electrical and Computer Engineering, the University of Wisconsin, Madison, WI 53706.

II. Statement of the Problem

A reactive surface occupying the plane $x=0$ and terminating the semi-infinite ($\infty>x>0$) dielectric medium has a reactance which has a sinusoidal variation in the z-direction as indicated in Fig. 1. Only plane guided waves

0018-9480/81/0600-0594$00.75